THE JOURNAL OF PHYSICAL CHEMISTRY B

Article

Cite This: J. Phys. Chem. B 2018, 122, 9443−9451

pubs.acs.org/JPCB

Site-Specific Incorporation of a Cu^{2+} Spin Label into Proteins for Measuring Distances by Pulsed Dipolar Electron Spin Resonance Spectroscopy

Gregory E. Merz, Peter P. Borbat, Alise R. Muok, Madhur Srivastava, David N. Bunck, Jack H. Freed,* and Brian R. Crane*

Department of Chemistry and Chemical Biology, Cornell University, Ithaca, New York 14853, United States

Supporting Information

ABSTRACT: Pulsed dipolar electron spin resonance spectroscopy (PDS) is a powerful tool for measuring distances in solution-state macromolecules. Paramagnetic metal ions, such as Cu^{2+}, are used as spin probes because they can report on metalloprotein features and can be spectroscopically distinguished from traditional nitroxide (NO)-based labels. Here, we demonstrate site-specific incorporation of Cu^{2+} into non-metalloproteins through the use of a genetically encodable non-natural amino acid, 3-pyrazolyltyrosine (PyTyr). We first incorporate PyTyr in cyan fluorescent protein to measure Cu^{2+}-to-NO distances and examine the effects of solvent conditions on Cu^{2+} binding and protein aggregation. We then apply the method to characterize the complex formed by the histidine kinase CheA and its target response regulator CheY. The X-ray structure of CheY−PyTyr confirms Cu labeling at PyTyr but also reveals a secondary Cu site. Cu^{2+}-to-NO and Cu^{2+}-to-Cu^{2+} PDS measurements of CheY−PyTyr with nitroxide-labeled CheA provide new insights into the conformational landscape of the phosphotransfer complex and have implications for kinase regulation.

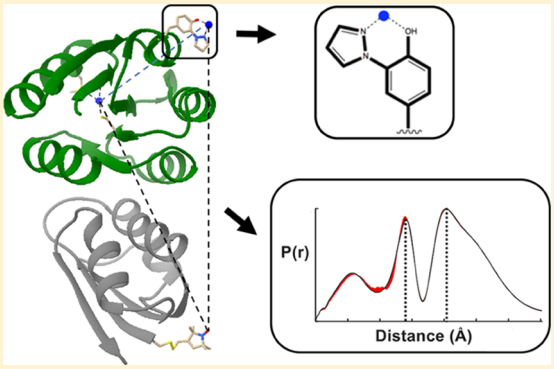

INTRODUCTION

Pulsed dipolar electron spin resonance (ESR) spectroscopy (PDS) in concert with site-specific spin labeling provides long-distance restraints (normally up to ∼90 Å,[1,2] but even longer in special cases[3]) to characterize protein conformation and assembly states in solution.[1,2,4] The most commonly used spin label is a nitroxyl-based spin-probe (NO), that is, covalently attached to engineered cysteine residues.[5] However, specific labeling of large proteins can be challenging as they often contain many Cys residues, not all of which can be replaced without altering critical properties. To circumvent this issue, non-natural amino acid incorporation has been developed for spin labeling.[6] However, the chemical stability of nitroxide radicals can be limiting, and furthermore, they are spectroscopically indistinguishable from each other. Thus, the presence of more than two sites creates complications in data interpretation.[7,8] The use of paramagnetic metal ions as spin probes for double electron−electron resonance (DEER) spectroscopy, both in conjunction with and in place of nitroxides, can mitigate these limitations. Anisotropic *g*-tensors of the metal ions allow for the specific excitation and detection of these centers, enabling metal−metal, metal−NO, and NO−NO interactions to be uniquely determined.[9−11] For example, Cu^{2+} ions have been used extensively in both proteins that natively bind the metal,[11−14] as well as protein and DNA systems that artificially incorporate Cu^{2+}.[15,16] PDS-derived distance distributions have also been obtained using manganese,[17,18] molybdenum,[19] and iron.[19−22] Recently, Gd^{3+} has been exploited as a spin label owing to its excitation at high frequency (W-band), which increases sensitivity.[23,24] Such sensitivity combined with genetically encoded specific labeling[25] opens the door to DEER measurements in vivo.[26] Nonetheless, specificity of binding is a major limitation in the use of metal ions as spin probes. Natural metal-binding centers in active sites and metal-binding loops of metalloproteins have been adopted to this end,[10−12,19,27,28] but engineering these complex centers into noncognate systems is not fully generalizable and can require substantial perturbations to the protein. A new semisynthetic strategy involving histidine placement in defined secondary structure offers minimum perturbation and transferability but still requires a specific scaffold.[28−30] Thus, a small, specific Cu^{2+} spin-probe that can be incorporated at any position in a protein is desirable. To this end, we have employed a genetically encodable non-natural derivative of tyrosine, 3-pyrazolyltyrosine (PyTyr, Figure 1), to site-specifically incorporate Cu^{2+} ions for PDS measurements. PyTyr was previously used as an electron acceptor in protein electron transfer experiments[31] and its

Received: June 12, 2018
Revised: September 7, 2018
Published: September 17, 2018

DOI: 10.1021/acs.jpcb.8b05619
J. Phys. Chem. B 2018, 122, 9443−9451

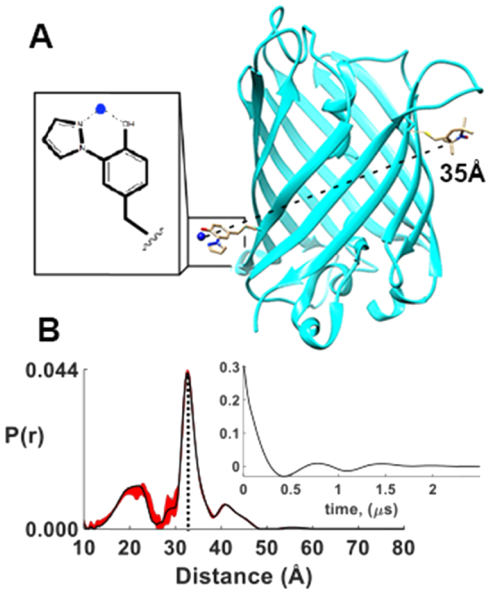

Figure 1. Targeted Cu^{2+} incorporation into CFP. (A) Cu^{2+} binding amino acid PyTyr shown with Cu^{2+}−NO separation in CFP expected from the crystal structure of CFP (PDB: 3ZTF[18]) modeled with a nitroxide on residue 208. (B) Distance distribution and denoised time-domain spectrum (inset) obtained by Cu^{2+}−NO DEER spectroscopy in H_2O-based buffer (see Figure S2 for D_2O data). The red regions indicate the small uncertainty arising from the SVD of the denoised signal.

ability to bind and stabilize Cu^{2+} with nanomolar affinity[31] makes it a suitable candidate for use as a spin label. Here, we incorporate PyTyr into two different proteins and demonstrate its utility for PDS. For proof of principle, we measure Cu^{2+}−NO distances in cyan fluorescent protein (CFP, Figure 1), and then, we characterize the interaction between the histidine kinase CheA and its phosphorylation target, the response regulator protein CheY (Figure 2).

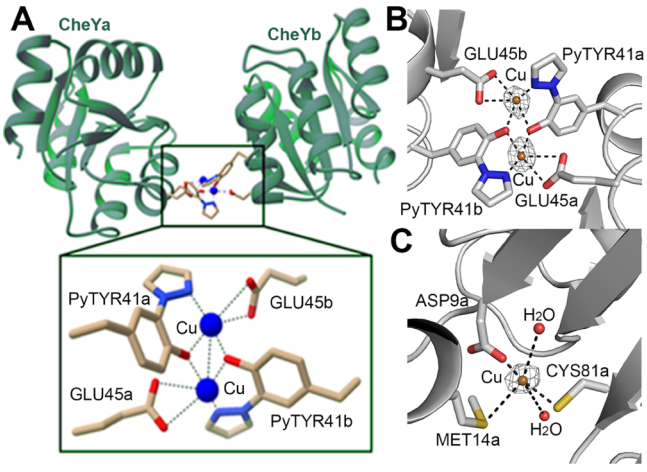

Figure 2. Crystal structure of CheY−PyTyr (A) ribbon representation of CheY41PyTyr. Inset: Cu center bridging the dimer; PyTyr sidechains serve as Cu ligands. (B) Unbiased electron density for di-Cu site at the dimer interface (B and D subunits), (C) unbiased electron density for the internal secondary Cu site. Refined omit map ($F_o - F_c$) electron density shown at 6σ for both (B,C).

EXPERIMENTAL METHODS

Synthesis of PyTyr. *Production of Boc-L-3-Iodotyrosine.* 3-Iodo-L-tyrosine was purchased from Aapptec. A 500 mL round bottom flask was charged with 3-iodo-L-tyrosine (2.0 g, 6.51 mmol), di-*tert*-butyl dicarbonate (1.42 g, 6.51 mmol), 40 mL of dioxane, and 60 mL of 500 mM NaOH. A solution of 6 M NaOH was then added dropwise until the pH reached 9.5. The reaction stirred at room temperature for 4 h. NaOH was added dropwise as needed to maintain the pH at 9.5. The reaction was quenched with 6 M HCl until the pH reached 1, at which time the solution was extracted with ethyl acetate and washed with 1 M HCl followed by brine. The organic layer was dried with $MgSO_4$ and filtered. Solvent was removed by rotary evaporation to afford a yellow oil. This oil was purified by column chromatography, using silica gel 60 Å with a gradient of dichloromethane/methanol (100/0 to 50/50 v/v). Drying under vacuum afforded an off-white solid (Boc-L-3-iodotyrosine) at 60% yield.

Production of PyTyr. Under a nitrogen atmosphere, Boc-L-3-iodotyrosine (2.0 g, 4.93 mmol) was added to a 100 mL Schlenk flask, along with Cs_2CO_3 (3.21 g, 9.86 mmol), CuI (0.47 g, 2.46 mmol), pyrazole (0.34 g, 4.93 mmol), and dry dimethylformamide (25 mL). The reaction was heated to 180 °C and was stirred for 18 h. After cooling, the reaction mixture was extracted with ethyl acetate and washed with 2 M HCl. The aqueous phase was concentrated by rotary evaporation to yield a brown solid. This solid was redissolved in water and then purified by high-performance liquid chromatography (Atlantis T3 C18 column 186003708, 40 mL/min flow rate, 0−60% acetonitrile in water over the course of 40 min) to a white solid at 15% yield. ^{1}H NMR (300 MHz DMSO-d_6): δ 8.34 (2H), 7.73 (1H), 7.62 (1H), 7.04 (2H), 6.51 (1H), 4.15 (1H), 3.08 (2H).

Protein Expression and Purification. DNA coding for the desired protein was cloned into pET28 using the NdeI and EcoRI restriction sites. For sequences cloned into the NdeI site, the histidine affinity tag introduced by the vector normally adds a GlySerHis peptide before the N-terminal Met residue. To guard against unwanted N-terminal copper binding, the His in this vector sequence was mutated to Ala after cloning into NdeI. The resulting plasmid was cotransformed with pEV01 containing PyTyrRS under control of an arabinose promoter in *Escherichia coli* BL21(DE3) cells. A single colony was picked and placed in a 5 mL starter culture of Luria−Bertani (LB) broth with kanamycin (250 μg/mL) and chloroamphenicol (170 μg/mL). After overnight growth at 37 °C, 1 mL of the starter culture was aliquoted into 200 mL of LB supplemented with the same concentration of antibiotics, as well as 30 mg of PyTyr. Cells were grown at 37 °C until the optical density reached an A_{600} of 0.6, at which time they were induced with isopropyl β-D-1-thiogalactopyranoside (1 mM final concentration) and arabinose (400 mg). The cells were grown at 37 °C overnight before being pelleted. The cell pellet was resuspended in 20 mL of lysis buffer [50 mM *N*-(2-hydroxyethyl)piperazine-*N*′-ethanesulfonic acid (HEPES) pH 7.5, 500 mM NaCl, and 5 mM imidazole], followed by sonication to lyse the cells. The lysate was then centrifuged, and the supernatant applied to Ni^{2+}−NTA affinity resin. Nonspecific binding was removed by washing with a buffer of 50 mM HEPES pH 7.5, 500 mM NaCl, and 20 mM imidazole (wash buffer). A solution of 5 mg [1-oxyl-2,2,5,5-tetramethyl-pyrroline-3-(methyl)-methanethiosulfate] (MTSSL), 150 μL

DOI: 10.1021/acs.jpcb.8b05619
J. Phys. Chem. B 2018, 122, 9443−9451

acetonitrile, and 5 mL wash buffer was added to the resin for labeling with a nitroxyl radical at position C208 or at both C208 and C151. This solution was incubated with the resin for 5 h at room temperature and then 7 h at 4 °C. The labeled protein was then eluted with a buffer of 50 mM HEPES pH 7.5, 500 mM NaCl, and 200 mM imidazole. The His_6 tag was removed by overnight incubation at room temperature with thrombin (200 μg), and the protein was further purified by size-exclusion chromatography (SEC) (Superdex 200 10/300 analytical column). Cu^{2+} was added by direct addition of $CuSO_4$ (1.5 equiv) and incubation at 4 °C overnight. The protein was then exchanged into a buffer of 50 mM (2-(*N*-morpholino)ethanesulfonic acid) (MES) pH 7.5, 150 mM NaCl, and 30% glycerol. This process yielded 830 μg of CFP151PyTyr. It was concentrated to 150 μM and flash-frozen for PDS measurements. Both D_2O-based buffers with d_8-deuterated glycerol and H_2O buffers with protonated glycerol were used as indicated. In some cases, 50 mM Tris-HCl [tris(hydroxymethyl)aminomethane hydrogen chloride] buffer pH 7.5 was used in place of MES to test the effects of a more strongly chelating buffer. *Thermotoga maritima* CheY41PyTyr was produced identically to that described above, except that Glu41 was mutated to TAG with QuikChange mutagenesis (Stratagene, La Jolla, CA). This process yielded 510 μg of CheY41PyTyr, which was concentrated to 600 μM, incubated with P_1P_2 as previously described, and then flash-frozen for PDS measurements. Selective and complete PyTyr incorporation was confirmed via electrospray ionization−mass spectrometry.

CheA P_1P_2 variants were expressed and purified as previously described,[7,32,33] and nitroxide labeling was performed in the same way as CFP above. The proteins were concentrated to 1 mM and flash-frozen for PDS measurements.

Structure Determination. CheY−41PyTyr−D54K crystals were obtained at 22 °C by the hanging drop vapor diffusion method by mixing 1.5 μL of CheY−41PyTyr−D54K in a buffer of 50 mM Tris-HCl pH 7.5 and 150 mM NaCl with 1.5 μL of mother liquor containing 100 mM HEPES pH 7.0, 200 mM $(NH_4)_2SO_4$, 22% poly(ethylene glycol) 4000, and 15 mM $CuCl_2$. Crystals were flash-frozen in liquid nitrogen. Diffraction data were collected at the 24-ID-C beamline of the Advanced Photon Source at Argonne National Laboratory at a wavelength of 0.979 Å with a Pilatus-6MF detector. Data were reduced and scaled using HKL2000.[34] The initial structure for CheY−41PyTyr−D54K was determined by molecular replacement using WT CheY (PDB ID: 4TMY) as a model. Further refinement was carried out with REFMAC[35] and PHENIX[36] amidst cycles of model building in COOT.[37]

SEC Coupled to Multi-Angle Light Scattering (SEC-MALS) of CheY−41PyTyr−D54K. To determine the oligomeric state of CheY−41PyTyr−D54K in solution, SEC-MALS was performed with and without Cu^{2+}. Proteins (2 mg/mL) were run at room temperature on an SEC column (SEC-s3000-BioSep) preequilibrated with 50 mM MES pH 7.5 and 150 mM NaCl buffer. The sample with Cu^{2+} was incubated overnight at 4 °C with 1 equiv of $CuSO_4$. Analysis and molecular weight determination were carried out with Wyatt technologies ASTRA. Bovine serum albumin (Sigma) was used as a control for data quality.

Pulsed Dipolar ESR Spectroscopy. *PDS Methods and Data Collection.* Briefly, in the standard (4-pulse) DEER method,[2] the sequence of three mw pulses, $\pi/2-t_1-\pi-t_2-\pi-(t_2-t_1)-$echo, is applied at the frequency ω_{detect} to create a refocused primary echo. This echo detects the electron spin at the selected field position in the ESR spectrum (of a Cu^{2+}), while the "pump" π-pulse, applied at a sufficiently different frequency, ω_{pump}, flips the electron spins corresponding to a different part of the spectrum, which can be that of another electron spin (of MTSSL e.g., referred to below as R1) at a distance *r*. The time position of the pump pulse is advanced in small (16 ns) steps from the second to the third detection pulse, producing an amplitude modulation of the echo by the dipole−dipole interaction between the electron spins. The modulation pattern thus mainly represents the "dipolar" oscillations from the coupling. From the oscillation frequency, $\omega_{dip} \propto 1/r^3$, the distance *r* can be accurately determined. The position of the echo does not change in this version of DEER; therefore, various relaxation and nuclear electron spin echo envelope modulation (ESEEM) contributions to the echo amplitude are relatively small residual effects.

Four-pulse DEER of CFP151PyTyr and CheY41PyTyr−CheA complexes was carried out on a modified home-built Ku-band, FT ESR spectrometer[38] operating over the 17.0−17.6 GHz frequency range and optimized for PDS.[39] The measurements were conducted on 100 μM protein solutions (usually deuterated, MES-buffered saline, and 30% glycerol) in 2 mm i.d. quartz capillary tubes at 20 K using a CF935 flow-cryostat with an ITC503A temperature controller (Oxford Instruments, Inc.). Figure S1 (right) shows the field-swept primary echo recorded on Cu^{2+}/R1 labeled CFP151PyTyr. The spectrum was recorded at 60 K at a pulse sequence repetition rate of 100 Hz to avoid power saturation of R1. At these conditions, the recorded spectrum is dominated by the narrow spectrum of R1; the Cu^{2+} part appears as a wide low-intensity band. The broad extent (~100 mT) of the Cu^{2+} ESR spectrum permits, in principle, a wide separation between the pump and detection frequencies in DEER measurements; thus, increased pulse intensities can be applied for nitroxides. However, in this work, the separation was limited by the resonator bandwidth to 140 MHz (≈5 mT). At the respective spectral position, the Cu^{2+} refocused echo is only a quarter of that at the spectral maximum at 600 mT but still affords a good signal-to-noise ratio (SNR).

For DEER detection on Cu^{2+}, we used an 8/16/16 ns pulse sequence applied at 1 kHz rate. The pump pulse in these cases was limited to 16 ns for Cu^{2+}−NO in order to keep small the nonlinear effects caused by simultaneous flipping of two NO spins (in the case of dimeric species), even though it was possible to flip more than 50% of the spins by using an 8 ns or shorter pumping pulse. In the $Cu^{2+}-Cu^{2+}$ distance measurements, the detection frequency was in the Cu^{2+} spectral region located 10 mT below the low-field edge of the nitroxide spectrum. An 8 ns pump pulse was applied 5 mT further below this point using 140 MHz higher microwave frequency. The signal background was approximated by a polynomial function in the semilog scale and subtracted out.[40] The modulation depth of the time-domain DEER spectrum (Δ) is defined as $\Delta(p) = \frac{\mathrm{DEER}_{(t=0)} - \mathrm{DEER}_{(t=\infty)}}{\mathrm{DEER}_{(t=0)}}$, where *p* is the fraction of spins flipped by the pump π-pulse.[41−44] Δ depends on the number of interacting spins, *N*, as $\Delta(p,N) = 1 - (1-p)^{N-1}$.[41−45] For two spins, $\Delta(p,2) = p$. We choose to plot the time domain data normalized to the modulation depth, such that $\mathrm{DEER}_{(t=0)} = \Delta$ and $\mathrm{DEER}_{(t=\infty)} = 0$. Under our experimental conditions (16 ns π-pulse pumped at the center of the nitroxide spectrum), Δ was ~0.36 for two sites that are 100% labeled. In the case of

DOI: 10.1021/acs.jpcb.8b05619
J. Phys. Chem. B 2018, 122, 9443−9451

Cu^{2+}, the pumping efficiency is <10% of that for nitroxide, but the pump pulse used was twice as intense (8 ns). Thus, one would expect Δ to be in the range of 0.03−0.10 for well-occupied Cu centers.

PDS Data and Error Analysis. To obtain well-resolved distance distribution, we first apply the WavPDS method[46] (a wavelet denoising procedure for PDS) to remove noise from the experimental signal. Noise in the PDS signal effectively restricts the resolution of the distance distribution. Unlike other filtering methods, the wavelet transform can simultaneously use both the time and frequency information to remove noise. The WavPDS method selects the threshold to eliminate noise without distorting the signal information,[47] thereby effectively retrieving the desired signal.

The denoised signal is then used to reconstruct distances using the new singular-value decomposition (SVD) method[48] developed to solve ill-posed problems such as for the PDS signal. The SVD method overcomes the limitations of the standard Tikhonov regularization method[49,50] in obtaining accurate distances and avoiding spurious peaks. Instead of finding a solution that is a compromise between stabilizing it in the presence of noise and obtaining a good approximation in regularization, the SVD method finds the optimal solution at each distance range from the denoised spectrum, leading to a well-resolved distribution. This method takes advantage of the fact that the $P(r)$ at each distance will converge with respect to the number of singular value contributions at different rates before becoming unstable.

After denoising, the SNR in this study is about 1000. Thus, unlike DEER studies processed by standard methods, the noise is not a primary source of uncertainty in the distance distribution.[51] What remains is the very small uncertainty in selection of the SVD cut-off[48] and uncertainty in the baseline subtraction. In the SVD method, accurate distributions are obtained from all the singular values that contribute to stable solutions. Different ranges of the distance distribution are treated independently. The uncertainty is estimated for singular value contributions, where the distance distribution has converged to the accurate solution and remains converged with added contributions. The minimum and maximum values that a distance range in the distribution can have in the converged region are taken as the uncertainty from this source.

Orientation Selections. Failure to account for insufficient sampling of the inter-spin angle in the Fredholm kernel due to Cu^{2+} *g*-factor anisotropy can skew distance distributions that result from a typical Tikhonov treatment of DEER data.[10,52] However, these errors are generally not large[10,11] and are further mitigated owing to the following factors that apply to the PDS data acquired here: (1) echo detection on the axial Cu(II) signal at high field values, where g_x and g_y are well excited and mixed into g_z from Cu(II) hyperfine splitting; (2) pump excitation captures virtually all of the nitroxide orientations to which a given observing Cu(II) center will be sensitive; and (3) unlike typical Cu-coordination centers, the Cu(II) label is flexible by virtue of pyTyr side-chain torsion angle variation. Hence, no special considerations were made for orientation selection effects caused by an observation frequency that did not cover the complete Cu(II) anisotropic *g*-tensor.

RESULTS AND DISCUSSION

Cu-Labeled Cyan Fluorescent Protein (CFP). In order to incorporate PyTyr into a protein of interest, we employed a mutant tRNA/tRNA synthetase pair (PyTyrRS) previously evolved to target the amber (TAG) stop codon.[31] PyTyr was synthesized from tyrosine and pyrazole by a cross-coupling reaction, with some modification to the published protocol (see Experimental Methods).[31] PyTyr was first incorporated into CFP (Figure 1), a derivative of green fluorescent protein that offers a colored, structurally characterized system to test protein yield and experimental feasibility.[53] PyTyr was placed at position 151 (CFP151PyTyr), and a Ser208Cys substitution was introduced by site-directed mutagenesis to allow additional labeling with a nitroxyl radical. This double mutant was cloned into pET28 and co-expressed with PyTyrRS in *E. coli* BL21(DE3) cells. The His_6-tagged protein was purified by Ni−NTA affinity chromatography, and Cys208 was labeled on-column with nitroxide spin label (MTSSL). After removal of the His-tag by thrombin digestion and subsequent gel filtration chromatography, the protein was buffer exchanged and concentrated to 100 μM for measurements. Finally, Cu^{2+} was added by incubation with $CuSO_4$ (1 equiv) at 4 °C overnight.

Cu^{2+}−NO PDS data were collected on 100 μM CFP in D_2O-based MES buffer over 12 h with a four-pulse DEER pulse sequence on a home-built Ku-band ESR spectrometer operating in the 17.0−17.6 GHz range.[38] For Cu^{2+}−NO measurements, nitroxide spins were pumped at 1 mT below the central maximum of the nitroxide spectrum, whereas Cu^{2+} spins were detected at a frequency corresponding to the field 5 mT below the pumped position (Figure S1). The time-domain trace (Figure S2) was first denoised with WavPDS[47] and then converted to distance distributions using the SVD method (see Experimental Methods).[48] This treatment was compared to that by Tikhonov regularization with maximum entropy optimization (TIKR-MEM, Figure S2). In both cases, the pairwise distance distribution obtained [$P(r)$, Figures 1B and S2] reveals a prominent peak at ∼35 Å that agrees well with a model based on the crystallographic structure of CFP (Figure 1),[54] but also a trailing shoulder at longer distances that likely represents a modest degree of aggregation owing to PyTyr-mediated interactions (see below). Both the TIKR-MEM and SVD treatments also give rise to a short-distance contribution at ∼20 Å. The dipolar frequency of this component is consistent with nuclear modulation from strongly coupled deuterons (ESEEM), which could derive from Cu^{2+}-coordinated solvent molecules that are observed in the crystal structure of pyTyr−CFP.[31] However, DEER data on a sample prepared in H_2O buffer (Figures 1B and S3) showed no change to the 20 Å feature, excluding ESEEM as primary explanation. Interestingly, the minor long distance components were reduced in H_2O, consistent with an origin in aggregation. We also prepared the sample in Tris-H_2O buffer, which is a stronger chelator of Cu^{2+} ($K_f \approx 10^8$)[55] than MES buffer, which does not bind cupric ion.[56] The considerably diminished signal produces a distribution in which the primary peak is maintained, but the short distance component is lost (Figure S3). This result suggests that the 20 Å feature may arise from a weakly bound Cu^{2+} ion.

To confirm that the longer distances may owe to protein aggregation, we collected DEER data so that both the pump and detection frequencies were set on nitroxide (NO−NO). As each CFP has only one R1 label, any NO−NO distances indicate some form of oligomerization (Figure S3). Indeed, an NO−NO distance of ∼47 Å is found, albeit the modulation depth is considerably less than in the Cu^{2+}−NO case (Figure S3). Finally, to corroborate the primary Cu^{2+}−NO distance

DOI: 10.1021/acs.jpcb.8b05619
J. Phys. Chem. B 2018, 122, 9443−9451

measurement, we also performed DEER on a CFP sample labeled at both positions 151 and 208 by R1 (Figure S3). This NO−NO experiment, where there are two nitroxide labels per monomer, gives a well-defined 34 Å distance with a broad base that agrees well with the primary peak of the Cu^{2+}−NO data (Figure S3). Thus, the PDS experiments with CFP demonstrate that the PyTyr incorporation allows Cu^{2+} targeting for determining distant constraints by DEER. Although complications from nonspecific Cu^{2+} binding and aggregation may arise, they are relatively minor effects in this case.

Histidine Kinase Response Regulator. PyTyr Cu^{2+}-labeling was then applied to characterize domain juxtaposition in the complex formed by the histidine kinase CheA and its response-regulator CheY. CheA and CheY form a two-component system that regulates bacterial motility in response to chemoattractants.[57] *T. maritima* CheA is a dimeric kinase, each subunit composed of five domains (named P1 through P5). CheY docks at the CheA P2 domain to receive phosphate from the P1 domain, which undergoes autophosphorylation on a specific histidine residue by the ATP-binding P4 domain. Flexible linkers allow P1 to interact with both P4 and P2-bound CheY.[58,59] Crystal and NMR structures are known for all of the CheA domains,[60−63] but the conformational properties of CheA, which are key for catalyzing phospho-transfer from ATP to CheY, are less well characterized. Following a protocol analogous to those described above, we labeled the response regulator CheY with PyTyr−Cu^{2+} at residue 41. In attempts to limit competitive Cu^{2+} binding by the CheY phosphorylation center,[64,65] which coordinates Mg^{2+}, Asp54 was changed to Lys. CheA domains P1P2 were labeled with nitroxide on either P1 (residue 76) or P2 (residue 178) in an otherwise Cys-less version of P1P2 (C63S, C208S, residues 1−263). CheY41PyTyr was expressed and purified (510 μg at 600 μM) in the same manner as CFP151PyTyr, except that there was no need for nitroxide spin labeling. Electron-spray ionization mass-spectrometry of CheY41PyTyr revealed the expected mass for incorporation of the non-natural amino-acid, with no contribution from CheY with the native residue at position 41 (Figure S4). CheA was expressed, purified, and spin-labeled, as previously described.[7] Complexes were formed by direct addition of each component and incubation overnight at 4 °C. Samples were flash-frozen in liquid N_2 for PDS measurements.

Structure of CheYPyTyr. To investigate copper binding to CheY41PyTyr and the effect of the PyTyr substitution on the CheY structure, we crystallized CheY41PyTyr with excess Cu^{2+} and determined the structure to 2.7 Å resolution (Table S1). Although CheY41PyTyr clearly binds Cu^{2+}, it does so through an unusual di-Cu coordination center at the interface of a crystallographic dimer (Figure 2). Each of the two Cu atoms is bound by the PyTyr sidechain and the carboxylate of Glu45, with the hydroxyl group of each PyTyr bridging the two metal atoms. This mode of metal coordination is decidedly different than that observed with PyTyrCFP.[31] To confirm that the di-Cu center of CheY41PyTyr forms as a consequence of crystallization, MALS was carried out to determine that the protein remains monomeric in solution (Figure S5). The molecular weight of CheY41PyTyr determined by MALS matched that for a CheY monomer (13.5 kDa), both in the presence and absence of one equivalent of Cu^{2+}. Thus, the dimeric structure found in the crystal structure of CheY−41PyTyr−D54K is a consequence of crystallization and/or the excess of Cu^{2+} and does not represent the primary species present in solution when only 1 equiv of Cu^{2+} is available. Nonetheless, under high concentrations, PyTyr-mediated di-Cu centers could produce some aggregation in the samples. Contributions from such dimers would be expected to generate small shoulders in the Cu^{2+}−NO distance distributions, as is observed with CFP (Figures 1, S2, and S3).

PDS of the CheY−CheA Complex. Cu^{2+}−NO DEER time-domain data (Figure S6) were collected and analyzed in the same manner as for CFP151PyTyr. The resulting distance distributions (Figure 3) report on the solution-state structure

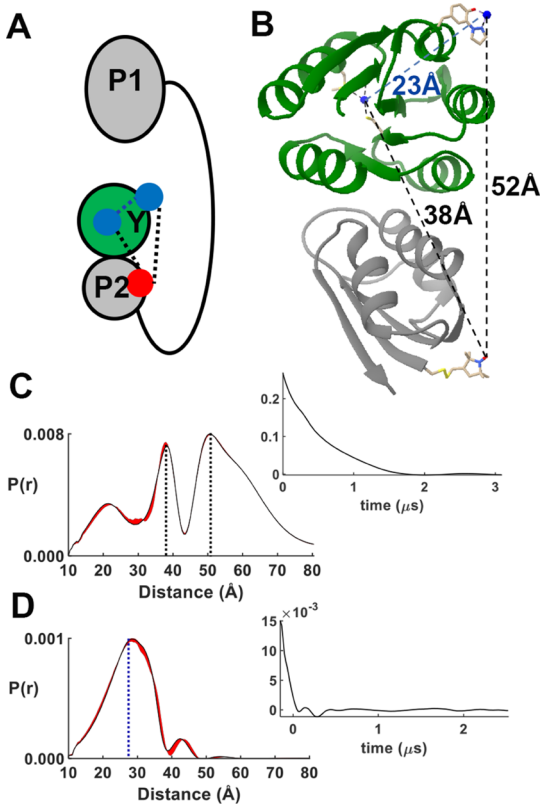

Figure 3. PyTyr-based PDS for the CheY−CheA P2 complex. (A) Schematic for CheY−P2 magnetic dipolar interactions. The copper centers of CheY are represented in blue, the nitroxide label in red. (B) Crystal structure of CheY in complex with the P2 domain of CheA (PDB: 1U0S[29]). The modeled Cu^{2+}−NO distances and Cu^{2+}−Cu^{2+} are in good agreement with the major peaks in the CheY−P2 distance distributions shown in (C,D). (C) Cu^{2+}−NO DEER-derived PDS distribution with its small uncertainty (red) for the CheY−P2 complex in D_2O buffer shown with background-corrected denoised time-domain data (inset). (D) Cu^{2+}−Cu^{2+} DEER-derived PDS distribution for the CheY−P2 complex shown with denoised time-domain data (inset).

of the CheA−CheY complex and can again be compared to crystallographic data. Interestingly, the Cu^{2+}−NO distance distribution between CheY and P2 has two dominant maxima, despite there being only one binding mode for the protein complex in the CheY−P2 crystal structure[32] (Figure 3B). The most probable distance of 52 Å in the major peak of the PDS distribution agrees well with that structure but the second peak, centered at 39 Å, does not. However, further analysis of the CheYPyTyr crystal structure revealed a second, more internal Cu^{2+} site involving Asp9, Met14, and Cys81 as coordinating ligands (Figure 2C). The predicted distance of

DOI: 10.1021/acs.jpcb.8b05619
J. Phys. Chem. B 2018, 122, 9443−9451

this second Cu^{2+} ion to the nitroxide label on P2 residue 178 is ~40 Å, which is consistent with the second major peak of the DEER distribution (Figure 3). Two Cu^{2+} ions within CheY should also produce a Cu^{2+}−Cu^{2+} dipolar signal. Indeed, such DEER results reveal a mean Cu^{2+}−Cu^{2+} separation of ~30 Å, again in keeping with the crystallographic coordinates (Figures 3 and S7). The modulation depth of the Cu^{2+} signal (Figure 3D) also suggests partial occupancy of this secondary site (Δ = 0.03−0.1 for two fully occupied sites, see Experimental Methods), again consistent with the crystallography. A short distance component may also contribute to the broad distribution derived from the Cu^{2+}−Cu^{2+} DEER data (Figure 3D). A possible metal-ion site on the surface of the protein ~15 Å from the internal Cu center was detected in the crystal structure; this surface position, which involves only Asp20 as a ligand, is unlikely to be highly occupied in the solvated complex. It is worth noting that the weak short distance component in the Cu^{2+}−NO distribution at ~20 Å (Figure 2C) does not arise from a Cu^{2+}−Cu^{2+} interaction and thus does not correspond to the 28 Å feature observed in the Cu^{2+}−Cu^{2+} distribution (Figure 3D). There is little intensity in the Cu^{2+} spectrum at the nitroxide pumping frequency (Figure S1), and furthermore, with a 16 ns pulse, the Cu^{2+} pumping efficiency is at least an order of magnitude less than that of nitroxide. Thus, Cu^{2+} pumping will be insignificant relative to that for nitroxide in the Cu^{2+}−NO dipolar spectrum. The source of the 20 Å peak in the Cu^{2+}−NO $P(r)$ is unclear but may involve a minor Cu^{2+} binding site in P2.

When the P1 domain is nitroxide-labeled, the resulting Cu^{2+}−NO signal with CheY produces a bimodal distribution with the major peak centered at ~24 Å and a smaller peak centered at 49 Å (Figures 4 and S8). Thus, the P1 domain is in close vicinity of the P2−CheY complex, despite the presence of a flexible spacer of considerable length (48 residues) between them. Interactions between CheY and P1 are weak and have been difficult to characterize, but the ~24 Å separation corroborates a model of the P1−CheY−P2 encounter complex produced from NMR data on the *E. coli* proteins[63] (Figure 4B). In this configuration, both the PyTyr and the internal Cu^{2+} center give nearly equal distances to the P1 nitroxide. Neither the Cu center is compatible with the 52 Å distance found in the distribution (Figure 4C). Thus, the P1 domain may alternate between two conformations: a docked state that contacts CheY and participates in phosphotransfer and an undocked state located further away from P2−CheY. Interactions of the domains or linker must constrain the undocked state at ~50 Å, roughly the distance across P1 and CheY. Colocalization of the undocked domains is also consistent with the inability of shorter linkers to increase autophosphorylation, which would be expected if P1 and P2 were joined but relatively unconstrained.[66] Localization of P1 by P2 will facilitate phosphotransfer to CheY, but not phosphorylation of P1 by P4. Thus, factors influencing the organization of the domains involved in phosphotransfer may have important implications for overall kinase regulation.

CONCLUSIONS

This study has demonstrated the site-specific incorporation of Cu^{2+} for use as a spin label in PDS experiments. In principle, any position on any protein expressed in *E. coli* can be targeted by this method. A clear issue is nonspecific binding of Cu^{2+} ion. For the CFP system, secondary Cu^{2+} binding was relatively minor and revealed by a more strongly chelating

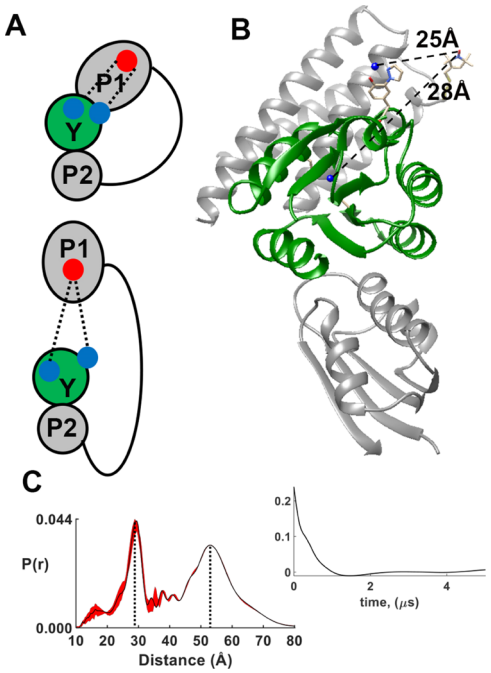

Figure 4. Phosphotransfer complex revealed by PyTyr PDS. (A) Schematic of the undocked (top) and docked (bottom) states of P1 relative to the P2−CheY complex. The copper centers of CheY are represented in blue, the nitroxide label in red. (B) Structural model of the docked state based on NMR data on *E. coli* proteins.[24] (C) Distance distribution for Cu^{2+}−NO (P1) DEER in H_2O with its small uncertainty (red) shows separations indicative of both major undocked and minor docked states. Both CheY Cu^{2+} centers give similar distances to the P1 nitroxide moiety in the docked configuration. Background-corrected denoised time-domain data displayed as an inset.

buffer. For CheY, an additional metal-ion binding site within the protein supplied two soft ligands (Met14 and Cys81), along with Asp9 to coordinate Cu^{2+}. However, such additional Cu^{2+} binding sites need not be detrimental to a structural study if they can be identified by other means, such as crystallography or Cu^{2+}−Cu^{2+} PDS. In the latter case, PyTyr incorporation can be used to detect such sites in the absence of other information. Another potential complication of Cu^{2+}−PyTyr is the tendency of the metal ion to complete its coordination shell with solvent or protein ligands. In D_2O, deuterium nuclear modulation from coordinated solvent has the potential to produce short distance components in $P(r)$. However, such effects were absent in these studies and nevertheless may be avoided by using H_2O buffers. Additional protein ligand coordination to the PyTyr metal complex can drive association, although the resulting higher-order species appear to be present in only minor amounts. Thus, with careful application, PyTyr incorporation extends PDS as a useful tool for exploring dynamic protein systems that are otherwise difficult to structurally characterize. The genetically encodable nature of PyTyr bypasses the need for attachment chemistry and overcomes issues such as protein degradation during labeling and the difficulty of targeting specific Cys residues in large proteins. Spectroscopic challenges of Cu^{2+} are also not necessarily limiting[10,11,67] and in some cases can be turned to advantage. We note that PyTyr is a derivative of Tyr, and where such a substitution is made, perturbation to the protein structure may not be large. Saxena et al. have described an

DOI: 10.1021/acs.jpcb.8b05619
J. Phys. Chem. B 2018, 122, 9443−9451

alternative strategy for incorporating Cu^{2+} specifically into proteins through introduction of judiciously positioned His residues on known secondary structure elements.[28−30] The combination of that strategy along with application of PyTyr will enable high-fidelity dual labeling with Cu^{2+}. Looking forward, the ability to genetically encode PyTyr Cu^{2+} labels, the precursors for which are generally less reactive than those for nitroxide radicals, also raises the possibility of their use as in vivo spin probes.

■ ASSOCIATED CONTENT

Supporting Information

The Supporting Information is available free of charge on the ACS Publications website at DOI: 10.1021/acs.jpcb.8b05619.

DEER data collection frequencies; DEER data analysis; time domain DEER data; solvent dependence of DEER data; Cu−NO versus NO DEER data, mass-spectrometry data for CheY−PyTyr; MALS data for CheY−PyTyr; and crystallographic statistics (PDF)

■ AUTHOR INFORMATION

Corresponding Authors

*E-mail: Jhf3@cornell.edu (J.H.F.).

*E-mail: bc69@cornell.edu. Phone: 607-254-8634 (B.R.C.).

ORCID

David N. Bunck: 0000-0002-6246-9846

Jack H. Freed: 0000-0003-4288-2585

Brian R. Crane: 0000-0001-8234-9991

Author Contributions

The manuscript was written through the contributions of all authors. All authors have given approval of the final version of the manuscript.

Notes

The authors declare no competing financial interest.

■ ACKNOWLEDGMENTS

This research was supported by NIH grants R01GM066775, R01GM079679, R35GM122535 (B.R.C.), P41GM103521 (J.H.F.), and Molecular Biophysics Training Grant T32GM008267 (G.E.M.). We thank NE-CAT at the Advanced Photon Source for access to data collection facilities (NIH grants P30 GM124165 and S10 RR029205). We would also like to thank Dr. Jiangyun Wang for providing us with the plasmid encoding PyTyrRS and T. K. Chua for help with crystallographic refinement and figure preparation.

■ REFERENCES

(1) Borbat, P. P.; Freed, J. H. Measuring distances by pulsed dipolar ESR spectroscopy: Spin-labeled histidine kinases. *Methods Enzymol.* **2007**, *423*, 52−116.

(2) Jeschke, G. DEER Distance Measurements on proteins. *Annu. Rev. Phys. Chem.* **2012**, *63*, 419−446.

(3) Schmidt, T.; Wälti, M. A.; Baber, J. L.; Hustedt, E. J.; Clore, G. M. Long distance measurements up to 160 angstrom in the GroEL tetradecamer using Q-band DEER EPR spectroscopy. *Angew. Chem., Int. Ed.* **2016**, *55*, 15905−15909.

(4) Crane, B. R.; Borbat, P. P.; Freed, J. H. Defining protein complexes that mediate bacterial chemotaxis by pulsed dipolar ESR spectroscopy. *Biophys. J.* **2014**, *106*, 685A.

(5) Hubbell, W. L.; Gross, A.; Langen, R.; Lietzow, M. A. Recent advances in site-directed spin labeling of proteins. *Curr. Opin. Struct. Biol.* **1998**, *8*, 649−656.

(6) Fleissner, M. R.; Brustad, E. M.; Kalai, T.; Altenbach, C.; Cascio, D.; Peters, F. B.; Hideg, K.; Peuker, S.; Schultz, P. G.; Hubbell, W. L. Site-directed spin labeling of a genetically encoded unnatural amino acid. *Proc. Natl. Acad. Sci. U.S.A.* **2009**, *106*, 21637−21642.

(7) Bhatnagar, J.; Borbat, P. P.; Pollard, A. M.; Bilwes, A. M.; Freed, J. H.; Crane, B. R. Structure of the Ternary complex formed by a chemotaxis receptor signaling domain, the CheA histidine kinase, and the coupling protein CheW as determined by pulsed dipolar ESR spectroscopy. *Biochemistry* **2010**, *49*, 3824−3841.

(8) Giannoulis, A.; Ward, R.; Branigan, E.; Naismith, J. H.; Bode, B. E. PELDOR in rotationally symmetric homo-oligomers. *Mol. Phys.* **2013**, *111*, 2845−2854.

(9) Bode, B. E.; Plackmeyer, J.; Prisner, T. F.; Schiemann, O. PELDOR measurements on a nitroxide-labeled Cu(II) porphyrin: Orientation selection, spin-density distribution, and conformational flexibility. *J. Phys. Chem. A* **2008**, *112*, 5064−5073.

(10) Yang, Z.; Kise, D.; Saxena, S. An approach towards the measurement of nanometer range distances based on Cu2+ ions and ESR. *J. Phys. Chem. B* **2010**, *114*, 6165−6174.

(11) Merz, G. E.; Borbat, P. P.; Pratt, A. J.; Getzoff, E. D.; Freed, J. H.; Crane, B. R. Copper-based pulsed dipolar ESR spectroscopy as a probe of protein conformation linked to disease states. *Biophys. J.* **2014**, *107*, 1669−1674.

(12) Evans, E. G. B.; Pushie, M. J.; Markham, K. A.; Lee, H.-W.; Millhauser, G. L. Interaction between prion protein's copper-bound octarepeat domain and a charged C-terminal pocket suggests a mechanism for N-terminal regulation. *Structure* **2016**, *24*, 1057−1067.

(13) van Wonderen, J. H.; Kostrz, D. N.; Dennison, C.; MacMillan, F. Refined distances between paramagnetic centers of a multi-copper nitrite reductase determined by pulsed EPR (iDEER) spectroscopy. *Angew. Chem., Int. Ed. Engl.* **2013**, *52*, 1990−1993.

(14) Yang, Z.; Kurpiewski, M. R.; Ji, M.; Townsend, J. E.; Mehta, P.; Jen-Jacobson, L.; Saxena, S. ESR spectroscopy identifies inhibitory Cu2+ sites in a DNA-modifying enzyme to reveal determinants of catalytic specificity. *Proc. Natl. Acad. Sci. U.S.A.* **2012**, *109*, E993−E1000.

(15) Cunningham, T. F.; Putterman, M. R.; Desai, A.; Horne, W. S.; Saxena, S. The double-histidine Cu(2)(+)-binding motif: a highly rigid, site-specific spin probe for electron spin resonance distance measurements. *Angew. Chem., Int. Ed. Engl.* **2015**, *54*, 6330−6334.

(16) Yang, Z.; Kise, D.; Saxena, S. An approach towards the measurement of nanometer range distances based on Cu2+ ions and ESR. *J. Phys. Chem. B* **2010**, *114*, 6165−6174.

(17) Martorana, A.; Yang, Y.; Zhao, Y.; Li, Q.-F.; Su, X.-C.; Goldfarb, D. Mn(II) tags for DEER distance measurements in proteins via C-S attachment. *Dalton Trans.* **2015**, *44*, 20812−20816.

(18) Meyer, A.; Schiemann, O. PELDOR and RIDME measurements on a high-spin manganese(II) bisnitroxide model complex. *J. Phys. Chem. A* **2016**, *120*, 3463−3472.

(19) Astashkin, A. V.; Rajapakshe, A.; Cornelison, M. J.; Johnson-Winters, K.; Enemark, J. H. Determination of the distance between the Mo(V) and Fe(III) heme centers of wild type human sulfite oxidase by pulsed EPR spectroscopy. *J. Phys. Chem. B* **2012**, *116*, 1942−1950.

(20) Le Breton, N.; Wright, J. J.; Jones, A. J. Y.; Salvadori, E.; Bridges, H. R.; Hirst, J.; Roessler, M. M. Using hyperfine electron paramagnetic resonance spectroscopy to define the proton-coupled electron transfer reaction at Fe-S cluster N2 in respiratory complex I. *J. Am. Chem. Soc.* **2017**, *139*, 16319−16326.

(21) Motion, C. L.; Lovett, J. E.; Bell, S.; Cassidy, S. L.; Cruickshank, P. A. S.; Bolton, D. R.; Hunter, R. I.; El Mkami, H.; Van Doorslaer, S.; Smith, G. M. DEER sensitivity between iron centers and nitroxides in heme-containing proteins improves dramatically using broadband, high-field EPR. *J. Phys. Chem. Lett.* **2016**, *7*, 1411−1415.

(22) Roessler, M. M.; King, M. S.; Robinson, A. J.; Armstrong, F. A.; Harmer, J.; Hirst, J. Direct assignment of EPR spectra to structurally defined iron-sulfur clusters in complex I by double electron-electron resonance. *Proc. Natl. Acad. Sci. U.S.A.* **2010**, *107*, 1930−1935.

DOI: 10.1021/acs.jpcb.8b05619
J. Phys. Chem. B 2018, 122, 9443−9451

(23) Gordon-Grossman, M.; Kaminker, I.; Gofman, Y.; Shai, Y.; Goldfarb, D. W-Band pulse EPR distance measurements in peptides using Gd(3+)-dipicolinic acid derivatives as spin labels. *Phys. Chem. Chem. Phys.* **2011**, *13*, 10771−10780.
(24) Matalon, E.; Huber, T.; Hagelueken, G.; Graham, B.; Frydman, V.; Feintuch, A.; Otting, G.; Goldfarb, D. Gadolinium(III) spin labels for high-sensitivity distance measurements in transmembrane helices. *Angew. Chem., Int. Ed.* **2013**, *52*, 11831−11834.
(25) Mascali, F. C.; Ching, H. Y. V.; Rasia, R. M.; Un, S.; Tabares, L. C. Using genetically encodable self-assembling Gd-III spin labels to make in-cell nanometric distance measurements. *Angew. Chem., Int. Ed.* **2016**, *55*, 11041−11043.
(26) Yang, Y.; Yang, F.; Gong, Y.-J.; Chen, J.-L.; Goldfarb, D.; Su, X.-C. A Reactive, Rigid Gd(III) labeling tag for In-cell EPR distance measurements in proteins. *Angew. Chem., Int. Ed.* **2017**, *56*, 2914−2918.
(27) van Wonderen, J. H.; Kostrz, D. N.; Dennison, C.; MacMillan, F. Refined distances between paramagnetic centers of a multi-copper nitrite reductase determined by pulsed EPR (iDEER) spectroscopy. *Angew. Chem., Int. Ed.* **2013**, *52*, 1990−1993.
(28) Cunningham, T. F.; Putterman, M. R.; Desai, A.; Horne, W. S.; Saxena, S. The double-histidine Cu2+-binding motif: A highly rigid, site-specific spin probe for electron spin resonance distance measurements. *Angew. Chem., Int. Ed.* **2015**, *54*, 6330−6334.
(29) Ghosh, S.; Lawless, M. J.; Rule, G. S.; Saxena, S. The Cu2+-nitrilotriacetic acid complex improves loading of alpha-helical double histidine site for precise distance measurements by pulsed ESR. *J. Magn. Reson.* **2018**, *286*, 163−171.
(30) Lawless, M. J.; Ghosh, S.; Cunningham, T. F.; Shimshi, A.; Saxena, S. On the use of the Cu2+-iminodiacetic acid complex for double histidine based distance measurements by pulsed ESR. *Phys. Chem. Chem. Phys.* **2017**, *19*, 20959−20967.
(31) Liu, X.; Li, J.; Dong, J.; Hu, C.; Gong, W.; Wang, J. Genetic incorporation of a metal-chelating amino acid as a probe for protein electron transfer. *Angew. Chem., Int. Ed.* **2012**, *51*, 10261−10265.
(32) Park, S.-Y.; Beel, B. D.; Simon, M. I.; Bilwes, A. M.; Crane, B. R. In different organisms, the mode of interaction between two signaling proteins is not necessarily conserved. *Proc. Natl. Acad. Sci. U.S.A.* **2004**, *101*, 11646−11651.
(33) Park, S. Y.; Crane, B. R. Crystallization and preliminary X-ray crystallographic analysis of CheW from Thermotoga maritima: a coupling protein of CheA and the chemotaxis receptor. *Acta Crystallogr., Sect. F: Struct. Biol. Commun.* **2011**, *67*, 504−506.
(34) Otwinowski, Z.; Minor, W. Processing of X-ray diffraction data collected in oscillation mode. *Methods Enzymol.* **1997**, *276*, 307−326.
(35) Murshudov, G. N.; Vagin, A. A.; Dodson, E. J. Refinement of macromolecular structures by the maximum-likelihood method. *Acta Crystallogr., Sect. D: Biol. Crystallogr.* **1997**, *53*, 240−255.
(36) Afonine, P. V.; Grosse-Kunstleve, R. W.; Echols, N.; Headd, J. J.; Moriarty, N. W.; Mustyakimov, M.; Terwilliger, T. C.; Urzhumtsev, A.; Zwart, P. H.; Adams, P. D. Towards automated crystallographic structure refinement with phenix.refine. *Acta Crystallogr., Sect. D: Biol. Crystallogr.* **2012**, *68*, 352−367.
(37) Emsley, P.; Lohkamp, B.; Scott, W. G.; Cowtan, K. Features and development of Coot. *Acta Crystallogr., Sect. D: Biol. Crystallogr.* **2010**, *66*, 486−501.
(38) Borbat, P. P.; Crepeau, R. H.; Freed, J. H. Multifrequency two-dimensional Fourier transform ESR: An X/Ku-band spectrometer. *J. Magn. Reson.* **1997**, *127*, 155−167.
(39) Borbat, P. P.; Georgieva, E. R.; Freed, J. H. Improved sensitivity for long-distance measurements in biomolecules: five-pulse double electron-electron resonance. *J. Phys. Chem. Lett.* **2013**, *4*, 170−175.
(40) Borbat, P. P.; Mchaourab, H. S.; Freed, J. H. Protein structure determination using long-distance constraints from double-quantum coherence ESR: study of T4 lysozyme. *J. Am. Chem. Soc.* **2002**, *124*, 5304−5314.
(41) Bhatnagar, J.; Sircar, R.; Borbat, P. P.; Freed, J. H.; Crane, B. R. Self-association of the histidine kinase CheA as studied by pulsed dipolar ESR spectroscopy. *Biophys. J.* **2012**, *102*, 2192−2201.
(42) Bode, B. E.; Margraf, D.; Plackmeyer, J.; Dürner, G.; Prisner, T. F.; Schiemann, O. Counting the monomers in nanometer-sized oligomers by pulsed electron - Electron double resonance. *J. Am. Chem. Soc.* **2007**, *129*, 6736−6745.
(43) Georgieva, E. R.; Borbat, P. P.; Norman, H. D.; Freed, J. H. Mechanism of influenza A M2 transmembrane domain assembly in lipid membranes. *Sci. Rep.* **2015**, *5*, 11757.
(44) Milov, A. D.; Ponomarev, A. B.; Tsvetkov, Y. D. Electron electron double resonance in electron-spin echo-model biradical systems and the senstized photolysis of declalin. *Chem. Phys. Lett.* **1984**, *110*, 67−72.
(45) Georgieva, E. R.; Ramlall, T. F.; Borbat, P. P.; Freed, J. H.; Eliezer, D. Membrane-bound alpha-synuclein forms an extended helix: Long-distance pulsed ESR measurements using vesicles, bicelles, and rodlike micelles. *J. Am. Chem. Soc.* **2008**, *130*, 12856−12857.
(46) Srivastava, M.; Georgieva, E. R.; Freed, J. H. A new wavelet denoising method for experimental time-domain signals: Pulsed dipolar electron spin resonance. *J. Phys. Chem. A* **2017**, *121*, 2452−2465.
(47) Srivastava, M.; Anderson, C. L.; Freed, J. H. A new wavelet denoising method for selecting decomposition levels and noise thresholds. *IEEE Access* **2016**, *4*, 3862−3877.
(48) Srivastava, M.; Freed, J. H. Singular value decomposition method to determine distance distributions in pulsed dipolar electron spin resonance. *J. Phys. Chem. Lett.* **2017**, *8*, 5648−5655.
(49) Chiang, Y.-W.; Borbat, P. P.; Freed, J. H. The determination of pair distance distributions by pulsed ESR using Tikhonov regularization. *J. Magn. Reson.* **2005**, *172*, 279−295.
(50) Chiang, Y.-W.; Borbat, P. P.; Freed, J. H. Maximum entropy: A complement to Tikhonov regularization for determination of pair distance distributions by pulsed ESR. *J. Magn. Reson.* **2005**, *177*, 184−196.
(51) Edwards, T. H.; Stoll, S. A Bayesian approach to quantifying uncertainty from experimental noise in DEER spectroscopy. *J. Magn. Reson.* **2016**, *270*, 87−97.
(52) Junk, M. J. N.; Spiess, H. W.; Hinderberger, D. Characterization of the solution structure of human serum albumin loaded with a metal porphyrin and fatty acids. *Biophys. J.* **2011**, *100*, 2293−2301.
(53) Heim, R.; Tsien, R. Y. Engineering green fluorescent protein for improved brightness, longer wavelengths and fluorescence resonance energy transfer. *Curr. Biol.* **1996**, *6*, 178−182.
(54) Goedhart, J.; von Stetten, D.; Noirclerc-Savoye, M.; Lelimousin, M.; Joosen, L.; Hink, M. A.; van Weeren, L.; Gadella, T. W. J.; Royant, A. Structure-guided evolution of cyan fluorescent proteins towards a quantum yield of 93%. *Nat. Commun.* **2012**, *3*, 751.
(55) Brignac, P. J.; Mo, C. Formation constants and metal-to-ligand rations for TRIS(Hydroxymethyl)aminomethane-metal complexes. *Anal. Chem.* **1975**, *47*, 1465−1466.
(56) Tesmar, A.; Wyrzykowski, D.; Jacewicz, D.; Żamojć, K.; Pranczk, J.; Chmurzyński, L. Buffer contribution to formation enthalpy of copper(II)-bicine complex determined by isothermal titration calorimetry method. *J. Therm. Anal. Calorim.* **2016**, *126*, 97−102.
(57) Falke, J. J.; Piasta, K. N. Architecture and signal transduction mechanism of the bacterial chemosensory array: Progress, controversies, and challenges. *Curr. Opin. Struct. Biol.* **2014**, *29*, 85−94.
(58) Hazelbauer, G. L.; Falke, J. J.; Parkinson, J. S. Bacterial chemoreceptors: high-performance signaling in networked arrays. *Trends Biochem. Sci.* **2008**, *33*, 9−19.
(59) Kentner, D.; Sourjik, V. Spatial organization of the bacterial chemotaxis system. *Curr. Opin. Microbiol.* **2006**, *9*, 619−624.
(60) Bilwes, A. M.; Alex, L. A.; Crane, B. R.; Simon, M. I. Structure of CheA, a signal-transducing histidine kinase. *Cell* **1999**, *96*, 131−141.
(61) Park, S.-Y.; Quezada, C. M.; Bilwes, A. M.; Crane, B. R. Subunit exchange by CheA histidine kinases from the mesophile Escherichia coli and the thermophile Thermotoga maritima. *Biochemistry* **2004**, *43*, 2228−2240.

DOI: 10.1021/acs.jpcb.8b05619
J. Phys. Chem. B 2018, 122, 9443−9451

(62) Quezada, C. M.; Grădinaru, C.; Simon, M. I.; Bilwes, A. M.; Crane, B. R. Helical shifts generate two distinct conformers in the atomic resolution structure of the CheA phosphotransferase domain from Thermotoga maritima. *J. Mol. Biol.* **2004**, *341*, 1283−1294.
(63) Mo, G.; Zhou, H.; Kawamura, T.; Dahlquist, F. W. Solution structure of a complex of the histidine autokinase CheA with its substrate CheY. *Biochemistry* **2012**, *51*, 3786−3798.
(64) Lukat, G. S.; Goff, H. M. A nuclear magnetic resonance study of axial ligation for the reduced states of chloroperoxidase, cytochrome P-450cam, and porphinatoiron(II) thiolate complexes. *Biochim. Biophys. Acta* **1990**, *1037*, 351−359.
(65) Kar, L.; Matsumura, P.; Johnson, M. E. Bivalent-metal binding to CheY protein. Effect on protein conformation. *Biochem. J.* **1992**, *287*, 521−531.
(66) Greenswag, A. R.; Muok, A.; Li, X.; Crane, B. R. Conformational transitions that enable histidine kinase autophosphorylation and receptor array integration. *J. Mol. Biol.* **2015**, *427*, 3890−3907.
(67) Pratt, A. J.; Shin, D. S.; Merz, G. E.; Rambo, R. P.; Lancaster, W. A.; Dyer, K. N.; Borbat, P. P.; Poole, F. L., II; Adams, M. W. W.; Freed, J. H.; Crane, B. R.; Tainer, J. A.; Getzoff, E. D. Aggregation propensities of superoxide dismutase G93 hotspot mutants mirror ALS clinical phenotypes. *Proc. Natl. Acad. Sci. U.S.A.* **2014**, *111*, E4568−E4576.

DOI: 10.1021/acs.jpcb.8b05619
J. Phys. Chem. B 2018, 122, 9443−9451